

Interactive 3D Modeling with a Generative Adversarial Network

JERRY LIU, Princeton University

FISHER YU, Princeton University

THOMAS FUNKHOUSER, Princeton University

This paper proposes the idea of using a generative adversarial network (GAN) to assist a novice user in designing real-world shapes with a simple interface. The user edits a voxel grid with a painting interface (like Minecraft). Yet, at any time, he/she can execute a SNAP command, which projects the current voxel grid onto a latent shape manifold with a learned projection operator and then generates a similar, but more realistic, shape using a learned generator network. Then the user can edit the resulting shape and snap again until he/she is satisfied with the result. The main advantage of this approach is that the projection and generation operators assist novice users to create 3D models characteristic of a background distribution of object shapes, but without having to specify all the details. The core new research idea is to use a GAN to support this application. 3D GANs have previously been used for shape generation, interpolation, and completion, but never for interactive modeling. The new challenge for this application is to learn a projection operator that takes an arbitrary 3D voxel model and produces a latent vector on the shape manifold from which a similar and realistic shape can be generated. We develop algorithms for this and other steps of the SNAP processing pipeline and integrate them into a simple modeling tool. Experiments with these algorithms and tool suggest that GANs provide a promising approach to computer-assisted interactive modeling.

1 INTRODUCTION

There has been growing demand in recent years for interactive tools that allow novice users to create new 3D models of their own designs. Minecraft for example, has sold over 120 million copies, up from 20 million just two years ago.

Yet 3D modeling is difficult for novice users. Current modeling systems provide either a simple user interface suitable for novices (e.g., [Igarashi et al. 1999; Microsoft 2017]) or the ability to make arbitrary 3D models with the details and complexity of real-world objects (e.g., [Autodesk 2017a,b]). Achieving both is an open and fundamental research challenge.

In this paper, we investigate how to use Generative Adversarial Networks (GANs) [Goodfellow et al. 2014] to help novices create realistic 3D models of their own designs using a simple interactive modeling tool. 3D GANs have recently been proposed for generating distributions of 3D voxel grids representing a class of objects [Wu et al. 2016]. Given a latent vector (e.g., a 200-dimensional vector with random values), a 3D-GAN can produce a sample from a latent distribution of voxel grids learned from examples (see the right side of Figure 1). Previous work has used 3D GANs for object classification, shape interpolation, and generating random shapes [Wu et al. 2016]. However, they have never before been used for interactive 3D modeling; nor has any other generative deep network.

We propose a new interactive modeling approach in which a user can leverage the generational power of a 3D GAN within an interactive modeling tool designed for novices. The user iteratively paints voxels with a simple interface similar to Minecraft [Microsoft 2017] and then hits the “SNAP” button, which replaces the current voxel grid with a similar one generated by a 3D GAN.

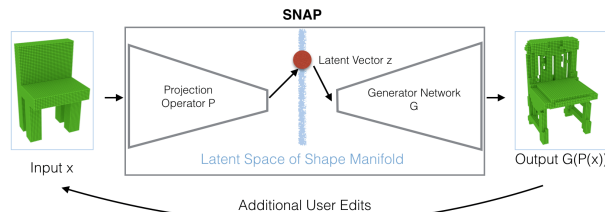


Fig. 1. Interactive 3D modeling with a GAN. The user iteratively makes edits to a voxel grid with a simple painting interface and then hits a SNAP command to refine the current shape. The SNAP command projects the current shape into a latent vector shape manifold learned with a GAN, and then generates a new shape with the generator network. These operations aim to increase the realism of the user’s input, while maintaining similarity to his/her inputs.

Figure 2 depicts an example workflow of this proposed approach. At the beginning, the user sketches the rough shape of an office chair (leftmost panel). When he/she hits the SNAP button, the system fills in the details of a similar chair generated with a 3D GAN (second panel). Then the user removes voxels corresponding to the top half of the back, which produces a new chair with a lower-back that might be used in a school setting. Finally, the user truncates the legs of the school chair, which then snaps to a lounge chair with a low base (note that the back becomes reclined to accommodate the short legs). In each case, the user provides approximate inputs with a simple interface, and the system produces a new shape sampled from a continuous distribution learned from real-world examples.

The main challenge in implementing such a system is to provide a projection operator $P(x)$ from a user-provided 3D voxel grid x to a feature vector z in the latent space of a 3D GAN such that the 3D voxel model x' generated by the GAN’s generator G from z is most similar to x (Figure 1). With such an operator, each SNAP operator can map x to $x' = G(P(x))$, ideally producing an output x' that is both similar to the input and representative of real-world objects in a given training set. To learn such an operator, we train a convolutional neural network (CNN) $z = P(x)$ for a pre-trained generator network $x' = G(z)$ with a loss function that balances the dissimilarity $D(x, x')$ between the input and output shapes and the unrealism $R(x')$ of the output shape relative to the whole generated distribution. We integrate this operator into an interactive model tool and demonstrate the effectiveness of the resulting SNAP command in several typical novice editing sessions.

The contributions of the paper are four-fold. First, it is the first to utilize a GAN in an interactive 3D model editing tool. Second, it proposes a novel way to project an arbitrary input into the latent space of a GAN, balancing both similarity to the input shape and

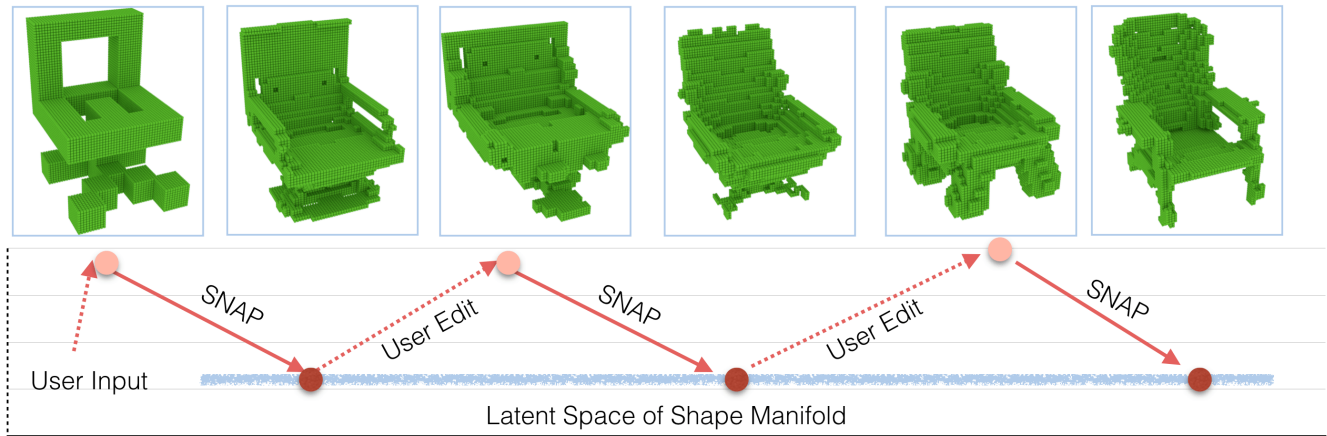


Fig. 2. A typical editing sequence. The user alternates between painting voxels (dotted arrows) and executing SNAP commands (solid arrows). For each SNAP, the system projects the current shape into a shape manifold learned with a GAN (depicted in blue) and synthesizes a new shape with a generator network.

realism of the output shape. Third, it provides a dataset of 3D polygonal models comprised of 101 object classes each with at least 120 examples in each class, which is the largest, consistently-oriented 3D dataset to date. Finally, it provides a simple interactive modeling tool for novice users.

2 RELATED WORK

There has been a rich history of previous works on using collections of shapes to assist interactive 3D modeling and generating 3D shapes from learned distributions.

Interactive 3D Modeling for Novices: Most interactive modeling tools are designed for experts (e.g., Maya [Autodesk 2017b]) and are too difficult to use for casual, novice users. To address this issue, several researchers have proposed simpler interaction techniques for specifying 3D shapes, including ones based on sketching curves [Igarashi et al. 1999], making gestures [Zelevnik et al. 1996], or sculpting volumes [Galyean and Hughes 1991]. However, these interfaces are limited to creating simple objects, since every shape feature of the output must be specified explicitly by the user.

3D Synthesis Guided by Analysis: To address this issue, researchers have studied ways to utilize analysis of 3D structures to assist interactive modeling. In early work, [Gal et al. 2009] proposed an “analyze-and-edit” to shape manipulation, where detected structures captured by wires are used to specify and constrain output models. More recent work has utilized analysis of part-based templates [Cashman and Fitzgibbon 2013; Kraevoy et al. 2009], stability [Averkiou et al. 2014], functionality [Sageman-Furnas et al. 2015], ergonomics [Zheng et al. 2016], and other analyses to guide interactive manipulation. Most recently, Yumer et al. [Yumer and Mitra 2016] used a CNN trained on un-deformed/deformed shape pairs to synthesize a voxel flow for shape deformation. However, each of these previous works is targeted to a specific type of analysis, a specific type of edit, and/or considers only one aspect of the design

problem. We aim to generalize this approach by using a learned shape space to guide editing operations.

Learned 3D Shape Spaces: Early work on learning shape spaces for geometric modeling focused on smooth deformations between surfaces. For example, [Kilian et al. 2007], [Allen et al. 2003], and others describe methods for interpolation between surfaces with consistent parameterizations. More recently, probabilistic models of part hierarchies [Huang et al. 2015; Kalogerakis et al. 2012] and grammars of shape features [Dang et al. 2015] have been learned from collections and used to assist synthesis of new shapes. However, these methods rely on specific hand-selected models and thus are not general to all types of shapes.

Learned Generative 3D Models: More recently, researchers have begun to learn 3D shape spaces for generative models of object classes using variational autoencoders [Brock et al. 2016; Girdhar et al. 2016; Sharma et al. 2016] and Generative Adversarial Networks [Wu et al. 2016]. Generative models have been tried for sampling shapes from a distribution [Girdhar et al. 2016; Wu et al. 2016], shape completion [Wu et al. 2015], shape interpolation [Brock et al. 2016; Girdhar et al. 2016; Wu et al. 2016], classification [Brock et al. 2016; Wu et al. 2016], 2D-to-3D mapping [Girdhar et al. 2016; Rezende et al. 2016; Wu et al. 2016], and deformations [Yumer and Mitra 2016]. 3D GANs in particular produce remarkable results in which shapes generated from random low-dimensional vectors demonstrate all the key structural elements of the learned semantic class [Wu et al. 2016]. These models are an exciting new development, but are unsuitable for interactive shape editing since they can only synthesize a shape from a latent vector, not from an existing shape. We address that issue.

GAN-based Editing of Images In the work most closely related to ours, but in the image domain, [Zhu et al. 2016] proposed using GANs to constrain image editing operations to move along a learned image manifold of natural-looking images. Specifically, they proposed a three-step process where 1) an image is projected into the latent image manifold of a learned generator, 2) the latent vector

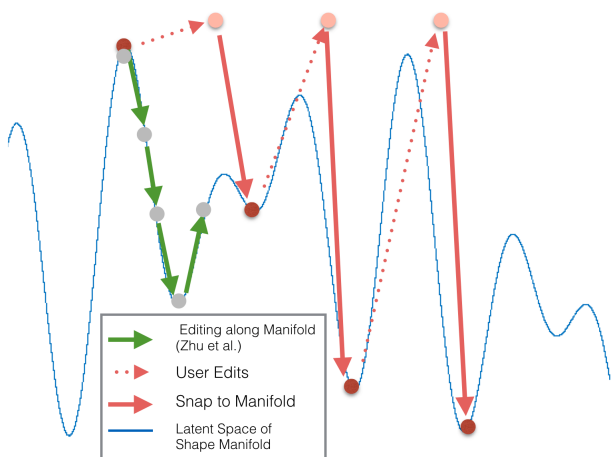


Fig. 3. Depiction of how the SNAP operators (solid red arrows) project edits made by a user (dotted red arrows) back onto the latent shape manifold (blue curve). In contrast, edits in Zhu et al. move to a local minimum (solid green arrows).

is optimized to match to user-specified image constraints, and 3) the differences between the original and optimized images produced by the generator are transferred to the original image. This approach provides the inspiration for our project. Yet, their method is not best for editing in 3D due to the modal structure of 3D shape spaces (e.g., a stool has either three legs or four, but never in between). Our contribution is to investigate how to utilize a GAN for editing in 3D, which requires a different approach.

3 APPROACH

In this paper, we investigate the idea of using a GAN to assist interactive modeling of 3D shapes.

During an off-line preprocess, our system learns a model for a collection of shapes within a broad object category represented by voxel grids (we have experimented so far with chairs, tables, and airplanes). The result of the training process is three deep networks, one driving the mapping from a 3D voxel grid to a point within the latent space of the shape manifold (the projection operator P), another mapping from this latent point to the corresponding 3D voxel grid on the shape manifold (the generator network G), and a third for estimating how real a generated shape is (the discriminator network D).

Then, during an interactive modeling session, a person uses a simple voxel editor to sketch/edit shapes in a voxel grid (by simply turning on/off voxels), hitting the “SNAP” button at any time to project the input to a generated output point on the shape manifold (Figure 2). Each time the SNAP button is hit, the current voxel grid x_t is projected to $z_{t+1} = P(x_t)$ in the latent space, and a new voxel grid x_{t+1} is generated with $x_{t+1} = G(z_{t+1})$. The user can then continue to edit and snap the shape as necessary until he/she achieves the desired output.

This general approach is related to that of Zhu et al. [Zhu et al. 2016] at a high level. However, their approach only supports edits

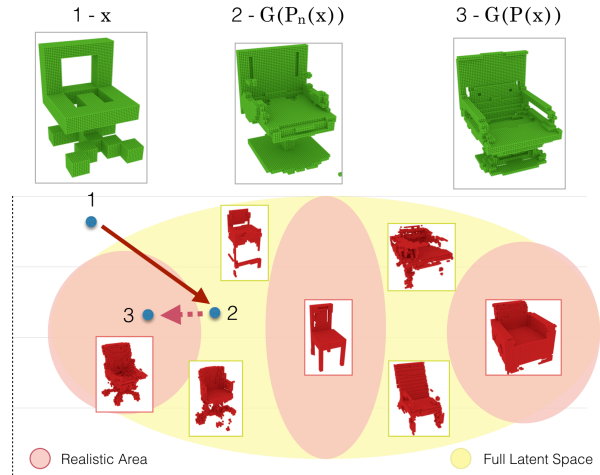


Fig. 4. Depiction of how subcategories separate within the latent shape space. Note that the shape space includes latent vectors z whose generator $G(z)$ produces an unrealistic shape (e.g., between subcategories). This is unavoidable when the shape space is structured. Our projection operator $z = P(x)$ is designed to avoid those regions.

that can be achieved by moving along the latent space to the nearest local minimum found with a gradient descent optimization. As a result, it would be difficult for them to support discrete or structural edits of the type required for 3D models (they support local color changes, contour placements, and deformations of images). In contrast, we allow users to make arbitrary edits to the voxel grid before projecting back to the latent space of the shape manifold with the SNAP operator (Figure 3). This approach supports structural edits as well as continuous ones, including adding/removing parts (e.g., adding arms to a chair) or switching between modes (e.g., from a table with four legs to one with a pedestal). Supporting these types of discrete edits would be difficult using a gradient descent optimization constrained to move along the latent space – a local minimum would almost surely be reached along the way (Figure 3).

Our approach is particularly well-suited for 3D modeling of real-world objects within broad categories. Since many object categories contain distinct subcategories (e.g., office chairs, dining chairs, reclining chairs, etc.) there are almost certainly modes within the shape space and regions between those that generate unrealistic objects (Figure 4). Our method allows users to make edits off the shape manifold before projecting back onto the manifold’s latent space; this allows us to define editing operations that jump over those unrealistic regions. Further, we can design our projection operator to avoid the unrealistic regions using the discriminator learned with the GAN, as described in Section 4.2. This key insight allows our editing system to generate objects that are simultaneously realistic and similar in shape to the input.

4 METHODS

This section describes each step of our process in detail. It start by describing the GAN architecture used to train the generator and discriminator networks. It then describes training of the projection

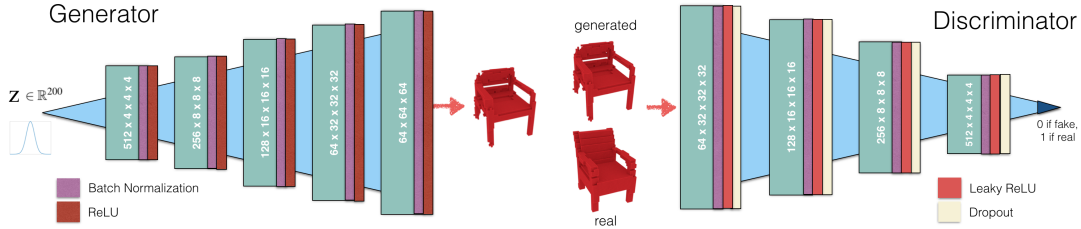


Fig. 5. Diagram of our 3D GAN architecture.

and classification networks. Finally, it describes implementation details of the interactive system.

4.1 Training the Generative Model

Our first preprocessing step is to train a generative model for 3D shape synthesis. We adapt the 3D-GAN model from [Wu et al. 2016], which consists of a generator G and discriminator D . G maps a 200-dimensional latent vector z to a $64 \times 64 \times 64$ cube, while D maps a given $64 \times 64 \times 64$ voxel grid to a binary output indicating real or fake (Figure 5).

We initially attempted to replicate [Wu et al. 2016] exactly, including maintaining the network structure, hyperparameters, and training process. However, we had to make adjustments to the structure and training process to maintain training stability and replicate the quality of the results in the paper. For instance, it is implied in the paper that G and D optimize the loss function in the following way:

$$\min_G \max_D \log D(x) + \log(1 - D(G(z)))$$

When we implemented this direct approach, the generator does not receive sufficient gradient from the discriminator, and training remains at a local minimum where the generator effectively outputs nothing. As a result we implemented the “trick” mentioned in the original Goodfellow paper [Goodfellow et al. 2014] which defines the generator-discriminator game to instead be:

$$\begin{aligned} & \max_G \log D(G(z)) \\ & \max_D \log D(x) + \log(1 - D(G(z))) \end{aligned}$$

Making the generator maximize $\log D(G(z))$ rather than minimizing $\log(1 - D(G(z)))$ provides much stronger gradients early on in training to prevent early collapse. Fixing the loss function solved the problem of immediate collapse and allowed the generator to generate shapes after several hundred epochs. But the generator still suffered from numerous issues. The outputs of the generator often-times collapsed to a very narrow distribution around a single output, a commonplace symptom due to the instability of GAN training. When the generated outputs did not collapse, they exhibited at most two modalities, rather than capturing the rich distribution of the different modes available within the training data.

To fix these issues we made additional adjustments to the network structure and training. Our generator is identical to the original, consisting of five full convolution layers with batch normalization and ReLU layers in between, and a sigmoidal output. Our discriminator is slightly different in that we added volumetric dropout

layers [Srivastava et al. 2014] of 50% after every LeakyReLU layer, but is otherwise identical. We found that adding dropout to the discriminator improved the stability of the generator and prevented it from collapsing at future epochs. The original paper also trained the generator by sampling from a uniform distribution in the range $[0, 1]$. We found that changing the sampling to be from a normal distribution $\mathcal{N}(0, I_{200})$ immediately increased the number of modalities of the output distribution as well as the visual quality of the samples.

We maintained the same hyperparameters, setting the learning rate of G to 0.0025, D to 10^{-5} , using a batch size of 100, and an Adam optimizer with $\beta = 0.5$. We initialize the convolutional layers using the method suggested by He et al. [He et al. 2015] for layers with ReLU activations.

4.2 Training the Projection Model

Our second step is to train a projection model $P(x)$ that produces a vector z within the latent space of our generator for a given input shape x . The implementation of this step is the trickiest and most novel of our system because it has to balance the following two considerations:

- The shape $G(z)$ generated from $z = P(x)$ should be “similar” to x . This consideration favors coherent edits matching the user input (e.g., if the user draws rough armrests on a chair, we would expect the output to be a similar chair with armrests).
- The shape $G(z)$ must be “realistic.” This consideration favors generating new outputs $x' = G(P(x))$ that are indistinguishable from examples in the GAN training set.

We balance these competing goals by optimizing an objective function with two terms:

$$\begin{aligned} P(x) &= \arg \min_z E(x, G(P(x))) \\ E(x, x') &= \lambda_1 D(x, x') + \lambda_2 R(x') \end{aligned}$$

where $D(x_1, x_2)$ represents the “dissimilarity” between any two 3D objects x_1 and x_2 , and $R(x)$ represents the “realism” of any given 3D object x (both are defined later in this section).

Conceptually, we can optimize the entire approximation objective E with its two components D and R at once. However, it is difficult to fine-tune λ_1, λ_2 to achieve robust convergence. In practice, it is easier to first optimize $D(x, x')$ to first get an initial approximation to the input, $z'_0 = P_5(x)$, and then use the result as an initialization to then optimize $R(G(z')) + D(x, G(z'))$ for a limited number of steps (implicitly setting $\lambda_1 = \lambda_2 = 1$). We can view the first step as optimizing for shape similarity and the second step as constrained

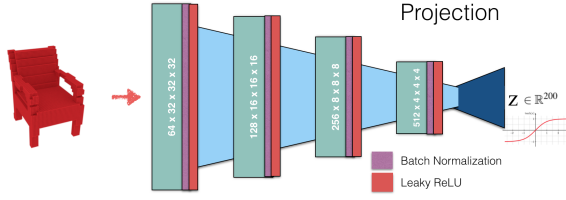


Fig. 6. Diagram of our projection network. It takes in an arbitrary 3D voxel grid as input and outputs the latent prediction in the generator manifold.

optimization for realism. With this process, we can ensure that $G(P(x))$ is realistic but does not deviate too far from the input.

$$P_S(x) \leftarrow \arg \min_z D(x, G(z)) | z = P(x)$$

$$P_R(z) \leftarrow \arg \min_{z'} R(G(z')) + D(x, G(z')) | z'_0 = P_S(x)$$

To solve the first objective, $P_S(x) = \arg \min_z D(x, G(z))$, there are numerous means of finding a solution. One option is to approximate it by sampling m points in the latent space of the generator and returning the point with the minimum dissimilarity – but this would be cost prohibitive. Another option is to use gradient descent as in [Zhu et al. 2016] – but this would find local minima (as noted in the previous section). Instead, we train a feedforward projection network $P_n(x, \theta_p)$ that predicts z from x , so $P_S(x) \leftarrow P_n(x, \theta_p)$. We allow P_n to learn its own projection function based on the training data. Since P_n maps any input object x to a latent vector z , the learning objective then becomes

$$\sum_{x_i \in X} \min_{\theta_p} D(x_i, G(P_n(x_i, \theta_p)))$$

where X represents the input dataset. The summation term here is due to the fact that we are using the same network P_n for all inputs in the training set as opposed to solving a separate optimization problem per input.

To solve the second objective,

$P_R(z) \leftarrow \arg \min_{z'} R(G(z')) + D(x, G(z'))$, we first initialize $z'_0 = P_S(x)$ (the point predicted from our projection network). We then optimize this step using gradient descent; in contrast to training P_n in the first step, we are fine with finding a local minima of $R(G(z')) + D(x, G(z'))$ so that we optimize for realism within a local neighborhood of the predicted shape approximation. The addition of $D(x, G(z'))$ to the objective adds this guarantee by penalizing the output shape if it is too dissimilar to the input.

Network Architecture: The architecture of P_n is given in Figure 6. It is mostly the same as that of the discriminator with a few differences. There are no dropout layers in P_n , and the last convolution layer outputs a 200-dimensional vector which is then passed through a tanh layer, representing the prediction of the latent vector z . One limitation with this approach is that $z \sim \mathcal{N}(0, 1)$, but since $P_n(x) \sim [-1, 1]^{200}$, the projection only learns a subspace of the generated manifold. We considered other approaches, such as removing the activation function entirely, but the quality of the projected results suffered; in practice, the subspace captures a significant portion of the generated manifold and is sufficient for most purposes.

During the training process, an input object x is forwarded through P_n to output z , which is then forwarded through G to output x' . Then we apply $D(x, x')$ to measure the distance loss between x and x' . Gradients are backpropagated through our distance function, then through G and then P_n ; however, note that we only update the parameters in P . Hence the training appears similar to training an autoencoder framework with some encoder and decoder and a custom reconstruction objective, except only the parameters of the encoder are updated. We did try training an end-to-end VAE-GAN architecture, as in Larsen et al. [Larsen et al. 2015], using our distance function as the reconstruction objective, but we were not able to tune the hyperparameters necessary to achieve better results than the ones trained with our method.

Dissimilarity Function: The dissimilarity function $D(x_1, x_2) \in \mathcal{R}$ is a differentiable metric representing the semantic difference between x_1 and x_2 . There are many possible choices. The simplest would be to use the L2 distance between the two voxel grids, but computing the L2 distance is expensive, and it is well-known that L2 is a poor measure of semantic dissimilarity. Instead, we aim to select a descriptor space where L2 distances are better approximations. One possible descriptor space is to take the intermediate activations from a 3D classifier network [Brock et al. 2016; Maturana and Scherer 2015; Qi et al. 2016; Su et al. 2015]. Another approach is to take the intermediate activations from the discriminator. We tried several approaches and found that the discriminator activations did the best job in capturing the important details of any category of objects, since they are specifically trained to distinguish between real and fake objects within a given category. We specifically select the output of the $256 \times 8 \times 8 \times 8$ layer in the discriminator (along with the Batch Normalization, Leaky ReLU, and Dropout layers on top) as our descriptor space. We denote this feature space as $conv15$ for future reference. We define $D(x_1, x_2)$ as $\|conv15(x_1) - conv15(x_2)\|$.

Realism Function: The realism function, $R(x) \in \mathcal{R}$, is a differential function that aims to estimate how indistinguishable a voxel grid x is from real object. There are many options for it, but the discriminator $D(x)$ learned with the GAN is a natural choice, since it is trained specifically for that task.

Training procedure: We train the projection network P_n with a learning rate of 0.0005 and a batch size of 50 using the same dataset used to train the generator. To increase generalization, we randomly drop 50% of the voxels for each input object - we expect that these perturbations allow the projection network to adjust to partial user inputs.

5 RESULTS

We have implemented a simple modeling tool based on the proposed approach and used it to run experiments with many types of shape edits. Since the modeling interface is extremely simple (turn on/off voxels under the cursor) and the generated results are not production quality (3D GANs are still in their infancy), we do not aim to test whether our prototype outperforms commercial systems in user tests (it would not). Rather, the goals of the experiments are to test the algorithmic components of the system and to demonstrate that 3D GANs can be useful in an interactive modeling tool for novices.

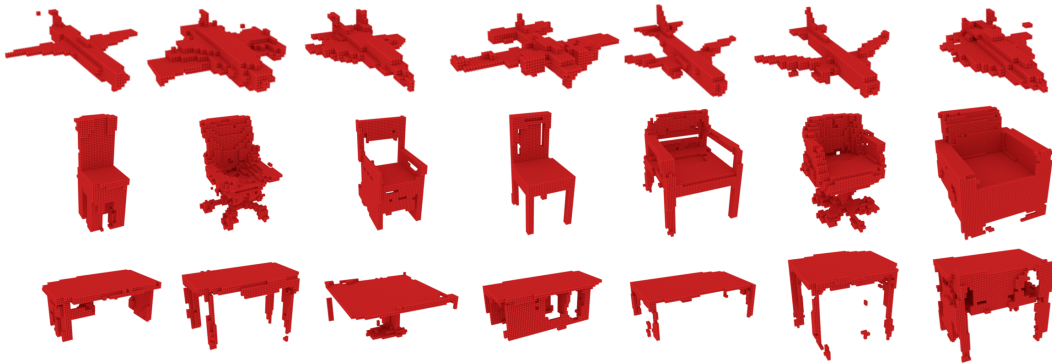


Fig. 7. Shapes generated from random latent vectors sampled from $\mathcal{N}(0, I_{200})$ using our 3D GANs trained separately on airplanes, chairs, and tables.

Our hope is to lay groundwork for future experiments on 3D GANs in an interactive editing setting.

5.1 Dataset

We curated a large dataset of 3D polygonal models for this project. The dataset is largely an extension of the ShapeNet Core55 dataset [Chang et al. 2015], but expanded by 30% via manual selection of examples from ModelNet40 [Wu et al. 2015], SHREC 2014 [Li et al. 2014], Yobi3D [Lee 2014] and a private ModelNet repository. It now covers 101 object categories (rather than 55 in ShapeNet Core55). The largest categories (chair, table, airplane, car, etc.) have more than 4000 examples, and the smallest now have at least 120 examples (rather than 56). The models are all aligned in the same scale and orientation.

We use the chair, airplane, and table categories for experiments in this paper. Those classes were chosen because they have the largest number of examples and exhibit the most interesting shape variations. The chairs exhibit numerous modalities, from upright stools to reclining chairs to wide couches. The airplanes range from fighter jets to commercial airliners to spaceships. The tables range from square to round table tops with a variety of leg heights.

5.2 Generation Results

We train our modified 3D-GAN on each category separately. Though quantitative evaluation of the resulting networks is difficult, we study the learned network behavior qualitatively by visualizing results.

Shape Generation: As a first sanity check, we visualize voxel grids generated by $G(z)$ when $z \in \mathbb{R}^{200}$ is sampled according to a standard multivariate normal distribution for each category. The results appear in Figure 7. They seem to cover the full shape space of each category, roughly matching the results in [Wu et al. 2016].

Shape Interpolation: In our second experiment, we visualize the variation of shapes in the latent space by shape interpolation. Given a fixed reference latent vector z_r , we sample six additional latent vectors $z_0, \dots, z_5 \sim \mathcal{N}(0, I_{200})$ and generate interpolations between z_r and z_i for $0 \leq i \leq 5$. The results are shown in Figure 8. The left-most image for row i represents $G(z_r)$, the right-most image represents $G(z_i)$, and each intermediate image represents some



Fig. 8. Shape Interpolation. The left image shows the reconstruction of a randomly sampled reference latent vector z_r . The right images show reconstructions for 6 other randomly sampled points, z_i . The middle images show reconstructions for in-betweens at uniformly spaced interpolations between z_r and z_i in the latent space.

$G(\lambda z_r + (1 - \lambda)z_i), 0 \leq \lambda \leq 1$. We make a few observations based on these results. The transitions between objects appear largely smooth - there are no sudden jumps between any two objects - and they also appear largely consistent - every intermediate image appears to be some interpolation between the two endpoint images. However, not every point on the manifold appears to be a valid object. For instance, some of the generated chairs are missing legs and other crucial features, or contain artifacts. This effect is particularly pronounced when z_r and z_i represent shapes with extra/missing parts or in different subcategories. For example, in row 4 of Figure 8, the midpoint between a stool and a comfortable chair with high armrests does not appear realistic. This result confirms the need for the realism term in our projection operation.



Fig. 9. Examples of chairs projected onto the generated manifold, with their generated counterparts shown as the output. The direct output of the projection network P_n is shown in the second row, while the output of the full projection function P is shown in the last row.

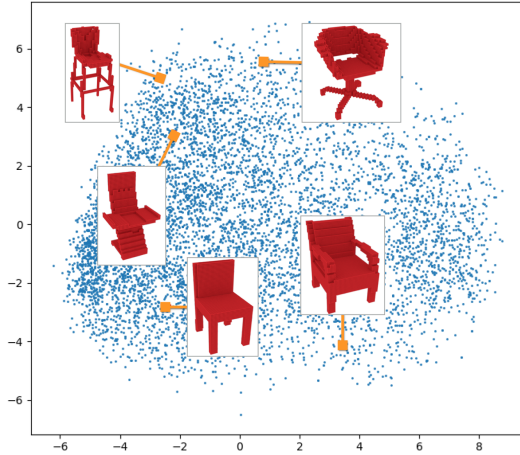


Fig. 10. 2-D PCA visualization of our training set of chairs projected onto the latent space of the chair generator.

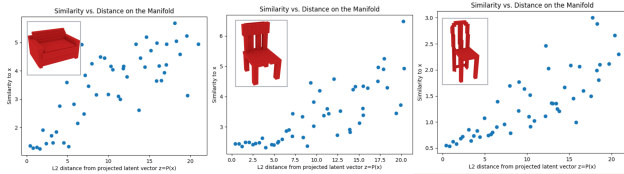


Fig. 11. Graph showing the correlation between the L2 distance in the latent space and the similarity measure $D(G(z), x)$. The horizontal axis shows L2 distances from $z = P(x)$, where x_0 is shown in the top-left of each plot and x is sampled from the training set. The vertical axis shows the similarity measure $D(G(z), x_0)$. Note that they are largely correlated.

5.3 Projection Results

In our next set of experiments, we investigate how well the projection operator predicts the latent vector for a given input shape. Figure 10 shows a PCA visualization of the distribution of $P_n(x)$ for each chair x . We observe a uniform distribution of projected latent points, which suggests that the projection network is able to learn a mapping to a broad subspace of the manifold and does not collapse to a localized region. Moreover, the relative absence of clusters suggests that the projection network does not merely memorize a few discrete modalities of the data.

Each projected vector $P_n(x)$ appears to find an optimum of the distance function within a wide local radius on the latent space with respect to the input x . This is demonstrated in Figure 11. We measure $D(G(z), x)$ with respect to the distance of z from $P(x)$. We sample various inputs from the training set. We note that $D(G(z), x)$ is still highly non-smooth and non-convex, but the projected point $P(x)$ is able to achieve a rough local minimum. This means that our projection network is adequately finding an approximately optimal point in the *conv15* feature space given an input.

A direct visual comparison of input and projected samples of chairs is demonstrated in Figure 9. An input chair x is provided in the first row (with many voxels missing). The second row shows the generated representation of the predicted latent vector from the projection network $P_n(x)$. The third row adds the second step of the projection function, which optimizes the latent vector towards a point $P(x)$ that would be classified as real by the discriminator.

On the whole, we see that the direct output of the projection network in the second row, $G(P_n(x))$, maintains the general visual features of the input. For instance, the height of the back in the first column, the shape of the armrests in the third column, as well as the width of the couch in the last column are preserved in the generated output. However, many of the generated images either contain missing components or contain extra artifacts which detract from the visual quality. The chairs in the 3rd and 4th images appear



Fig. 12. Voxel editing interface, adopted from Voxel Builder.

incomplete, while the chairs in the 7th and 8th images appear too noisy.

The output of the full projection operator shown in the third row address most of these issues. The second optimization step of the projection operator that pushes the predicted latent vector into a more realistic region of the manifold creates a noticeable improvement in the visual quality of the results overall. For example, in the second column, the final swivel chair looks more realistic and better match the style of the input than the fragmented prediction of the projection network alone. However, of course, there are cases where coercing realism moves the shape away from the user’s intended edit (e.g., the couch in the last column is transformed into a wide chair with armrests). The trade-off between realism and faithfulness to the user’s edit could be controlled with a slider presented to the user to address this issue.

6 SHAPE MANIPULATION APPLICATION

In this section, we describe how the 3D GAN and projection networks are integrated into an interactive 3D shape manipulation application.

The application is based upon an open-source Voxel Builder tool [Ogden 2015], which provides a user interface for easily creating and editing voxels in a grid (Figure 12). We customize the source code by removing the default editing operations and replacing them with a single SNAP button. When the user hits that button, the current voxel grid is projected into the latent shape manifold and then forwarded through the generator to create a new voxel grid that lies on the manifold. The user iterates between editing voxels and hitting the SNAP button until he/she is happy with the result.

The Snap operation is the foundation for our application. The processing is done in a server implemented in Node.js. The server triggers our external PyTorch scripts in order to feed the input through the projection and generator networks. Internally, the voxel grid is 64x64x64, but the Voxel Builder interface can only handle displays of 32x32x32 at interactive rates, and so the server upsamples the grid before passing it to the network and downsamples it for display in the Voxel Builder interface.



Fig. 13. Examples of projected outputs from various rough input sketches, along with the most similar retrieved object from the training set.

We postprocess the voxels on the server end before returning them to the user. This is an important step to improve the quality and realism of the generated results. Specifically, we remove small connected components of voxels from the output. For symmetric objects, we generate only half of the output and then synthesize the other half with a simple reflection. These simple steps improve both the speed and realism of the generated outputs.

The speed of a complete SNAP operation is around 9 seconds on average using an NVIDIA Tesla M40 GPU for the forward passes of the networks and gradient optimization steps. Of course, this is a bit too slow for a production-level interactive modeling tool. However, there are numerous ways to optimize the pipeline, such as maintaining the projector and generator in GPU memory rather than loading them from disk for every SNAP. We have not focused on speed in our prototype system because our goal is to investigate the idea of using a GAN for 3D modeling, not to provide a deployable system for commercial users.

Editing Sequence Results: Our final set of experiments show the types of edits that are possible with the assistance of a 3D GAN. In each experiment, we show a sequence of voxel edits followed by SNAP commands and then analyze whether/how the SNAP assists the user in creating detailed and realistic models of their own design.

Figure 13 shows a few example outputs from a single SNAP command. The top row shows the user input, the second row shows the snapped output, and the last row shows the closest retrieved object from the training data. In general, the results appear to preserve the general shape of the input (Wider input chairs yield wider output chairs, input chairs with longer legs yield output legs, and so forth). However, the snapped results generally fill in details missing in the inputs without replicating the training data.

Figure 14 shows several editing sequences comprising multiple voxel edits and SNAP commands. Results are shown for chairs, airplanes, and tables. For each editing sequence, the user starts by creating an object from scratch (left column), and then continues to edit the generated object by adding or removing voxels (magenta arrows) and then snapping (black arrows) for three iterations. We

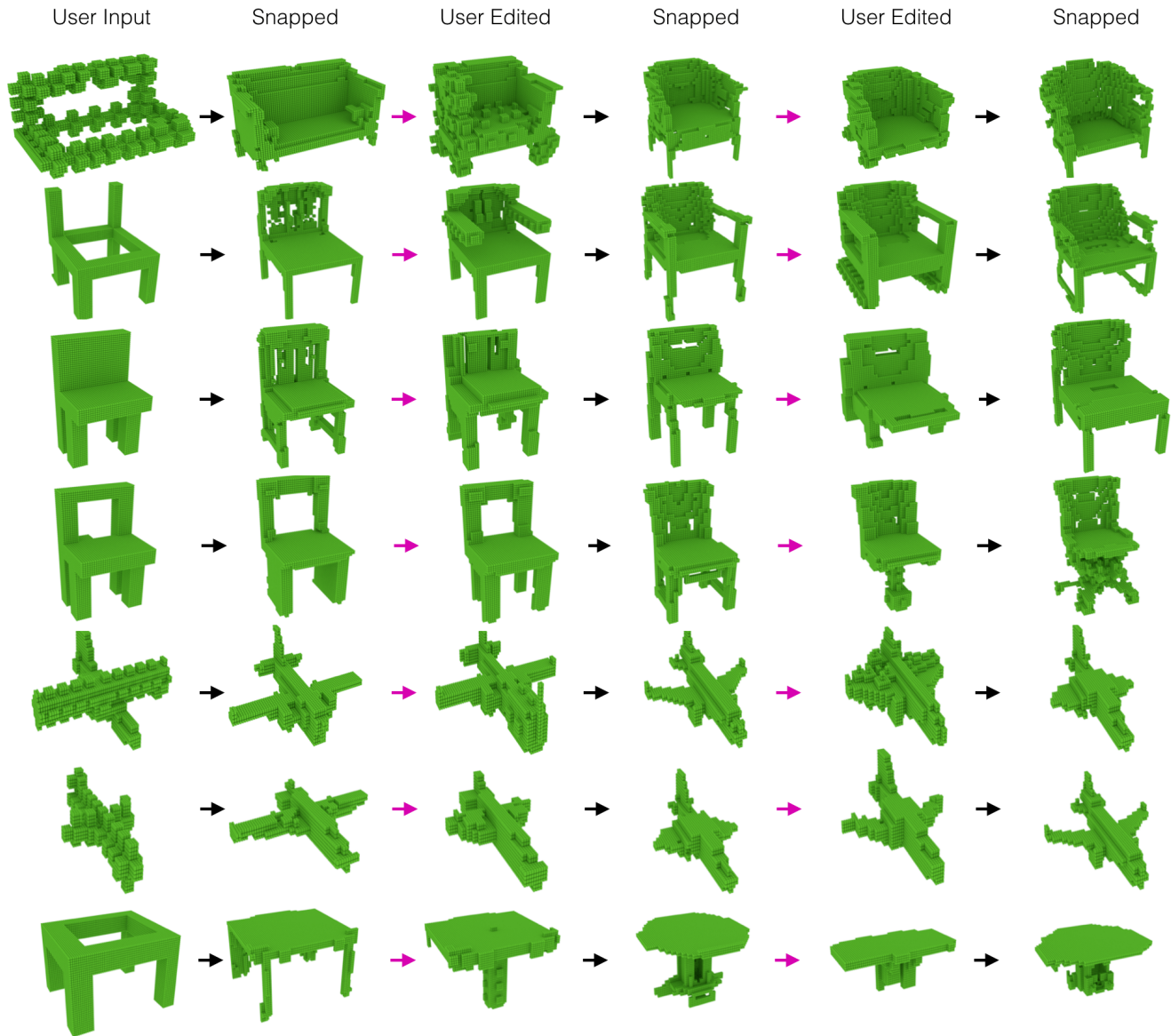


Fig. 14. Demonstration of editing sequences performed with our interface. The user paints an initial shape (left) and then alternates between snapping it (black arrows) and adding/removing voxels (magenta arrows). After each snap, the resulting object conforms roughly to the specifications of the user.

can see that the snapped objects are generally similar to their input, but more realistic representations of the object class. For example, it fills in the details of the couch in the first snap in the first row, and it fixes the aspect ratio of the chair in the last snap of the fourth row.

The snap operator often adjusts the overall style of the object to accommodate user edits. For example, in the first row, the user shrinks the width of the couch, and the snapped result is no longer rectangular - it becomes a fauteuil-esque chair with high armrests and a curved back. In the second row, the armrests that the user applies to the chair causes the overall structure of the back and legs

to change in the snapped output. Finally, as shown in the sixth row, shortening the wings of a plane causes the overall frame to transform into a sleek fighter jet. These examples suggest that our GAN-based editing approach is doing more than just shape completion; the process of snapping structural edits made by the user causes the entire structure of the object to change in order to remain on the shape manifold. A truncated, rectangular couch is not realistic (row 1), nor is the patterned back of an upright chair once the user adds armrests (row 2), nor are straight wings pushed to the middle of a plane (row 5). This implies that our approach is able to find a good balance between similarity and realism, returning results for the

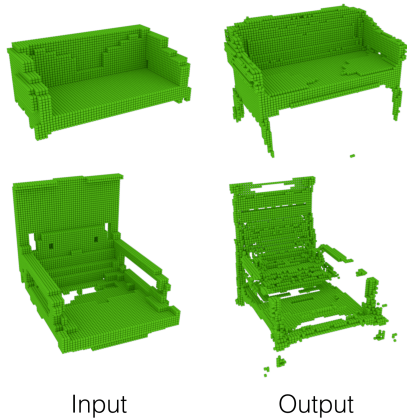


Fig. 15. Failure cases. The left column shows the user’s input, and the right column shows the result generated by our SNAP operator. Note that the result in the bottom row is unrealistic, and the result in the top row adds legs to what is intended as a sofa.

user that match both the edits made by the user as well as the style of a realistic object.

Failure Cases: There are some cases where the SNAP operator makes the result worse rather than better. It might produce results that are unrealistic (bottom row of Figure 15a), perhaps because the GAN has limited training data. Or, it might produce results dissimilar from the user intentions (top row of Figure 15), perhaps because realism is weighted too highly in the projection operator. These failures could be mitigated somewhat with more sophisticated validation and/or post-processing of generated outputs. We did not investigate such methods, as they would only mask the conclusions that can be made from our results.

7 CONCLUSION

In summary, we present a novel means of performing 3D shape manipulation by developing a framework of deep learning models around a deep generative model. We use 3D-GAN as our generative model, and design a projection function to project user input to a latent point in the manifold that both captures the input shape and appears realistic. In the process we employ our trained discriminator to provide a feature space as well as a measurement of realism which is essential towards improving the quality of our results. We’ve shown that editing operations with an easy-to-use interface can invoke complex shape manipulations adhering to the underlying distribution of shapes within a category.

This work is just a baby step in the direction of using generative adversarial networks to assist interactive 3D modeling. We have investigated the core issues in developing a system based on this idea, but it may be years before GAN-based systems produce outputs of quality high enough for production systems. Future work should develop better ways to learn projection and generation operators, and investigate alternative strategies for balancing trade-offs between matching user inputs and prior shape distributions.

REFERENCES

- Brett Allen, Brian Curless, and Zoran Popović. 2003. The space of human body shapes: reconstruction and parameterization from range scans. *ACM transactions on graphics (TOG)* 22, 3 (2003), 587–594.
- Autodesk. 2017a. Autodesk 3ds Max. (2017). <https://www.autodesk.com/products/3ds-max/overview>
- Autodesk. 2017b. Autodesk Maya. (2017). <https://www.autodesk.com/products/maya/overview>
- Melinos Averkiou, Vladimir G Kim, Youyi Zheng, and Niloy J Mitra. 2014. Shapessynth: Parameterizing model collections for coupled shape exploration and synthesis. *Computer Graphics Forum* 33, 2 (2014), 125–134.
- André Brock, Theodore Lim, James M. Ritchie, and Nick Weston. 2016. Generative and Discriminative Voxel Modeling with Convolutional Neural Networks. *CoRR* abs/1608.04236 (2016). <http://arxiv.org/abs/1608.04236>
- Thomas J. Cashman and Andrew W. Fitzgibbon. 2013. What Shape Are Dolphins? Building 3D Morphable Models from 2D Images. *IEEE Trans. Pattern Anal. Mach. Intell.* 35, 1 (Jan. 2013), 232–244. DOI: <http://dx.doi.org/10.1109/TPAMI.2012.68>
- Angel X. Chang, Thomas A. Funkhouser, Leonidas J. Guibas, Pat Hanrahan, Qi-Xing Huang, Zimo Li, Silvio Savarese, Manolis Savva, Shuran Song, Hao Su, Jianxiong Xiao, Li Yi, and Fisher Yu. 2015. ShapeNet: An Information-Rich 3D Model Repository. *CoRR* abs/1512.03012 (2015). <http://arxiv.org/abs/1512.03012>
- Minh Dang, Stefan Lienhard, Duygu Ceylan, Boris Neubert, Peter Wonka, and Mark Pauly. 2015. Interactive design of probability density functions for shape grammars. *ACM Transactions on Graphics (TOG)* 34, 6 (2015), 206.
- Ran Gal, Olga Sorkine, Niloy J Mitra, and Daniel Cohen-Or. 2009. iWIRES: an analyze-and-edit approach to shape manipulation. In *ACM Transactions on Graphics (TOG)*, Vol. 28. ACM, 33.
- Tinsley A Galyean and John F Hughes. 1991. Sculpting: An interactive volumetric modeling technique. In *ACM SIGGRAPH Computer Graphics*, Vol. 25. ACM, 267–274.
- Rohit Girdhar, David F. Fouhey, Mikel Rodriguez, and Abhinav Gupta. 2016. Learning a Predictable and Generative Vector Representation for Objects. *CoRR* abs/1603.08637 (2016). <http://arxiv.org/abs/1603.08637>
- I. J. Goodfellow, J. Pouget-Abadie, M. Mirza, B. Xu, D. Warde-Farley, S. Ozair, A. Courville, and Y. Bengio. 2014. Generative Adversarial Networks. *ArXiv e-prints* (June 2014). [arXiv:stat.ML/1406.2661](http://arxiv.org/abs/1406.2661)
- Kaiming He, Xiangyu Zhang, Shaoqing Ren, and Jian Sun. 2015. Delving Deep into Rectifiers: Surpassing Human-Level Performance on ImageNet Classification. *CoRR* abs/1502.01852 (2015). <http://arxiv.org/abs/1502.01852>
- Haibin Huang, Evangelos Kalogerakis, and Benjamin Marlin. 2015. Analysis and synthesis of 3D shape families via deep-learned generative models of surfaces. *Computer Graphics Forum* 34, 5 (2015).
- Takeo Igarashi, Satoshi Matsuoka, and Hidehiko Tanaka. 1999. Teddy: A Sketching Interface for 3D Freeform Design. In *Proceedings of the 26th Annual Conference on Computer Graphics and Interactive Techniques (SIGGRAPH '99)*. ACM Press/Addison-Wesley Publishing Co., New York, NY, USA, 409–416. DOI: <http://dx.doi.org/10.1145/311535.311602>
- Evangelos Kalogerakis, Siddhartha Chaudhuri, Daphne Koller, and Vladlen Koltun. 2012. A probabilistic model for component-based shape synthesis. *ACM Transactions on Graphics (TOG)* 31, 4 (2012), 55.
- Martin Kilian, Niloy J Mitra, and Helmut Pottmann. 2007. Geometric modeling in shape space. In *ACM Transactions on Graphics (TOG)*, Vol. 26. ACM, 64.
- Vladislav Kraevoy, Alla Sheffer, and Michiel van de Panne. 2009. Modeling from Contour Drawings. In *Proceedings of the 6th Eurographics Symposium on Sketch-Based Interfaces and Modeling (SBIM '09)*. ACM, New York, NY, USA, 37–44. DOI: <http://dx.doi.org/10.1145/1572741.1572749>
- Anders Boesen Lindbo Larsen, Søren Kaae Sønderby, and Ole Winther. 2015. Autoencoding beyond pixels using a learned similarity metric. *CoRR* abs/1512.09300 (2015). <http://arxiv.org/abs/1512.09300>
- Jessy Lee. 2014. Yobi3D. (2014). <https://www.yobi3d.com/>
- B. Li, Y. Lu, C. Li, A. Godil, T. Schreck, M. Aono, Q. Chen, N. K. Chowdhury, B. Fang, T. Furuya, H. Johan, R. Kosaka, H. Koyanagi, R. Ohbuchi, and A. Tatsuma. 2014. Large Scale Comprehensive 3D Shape Retrieval. In *Proceedings of the 7th Eurographics Workshop on 3D Object Retrieval (3DOR '15)*. Eurographics Association, Aire-la-Ville, Switzerland, Switzerland, 131–140. DOI: <http://dx.doi.org/10.2312/3dor.20141059>
- D. Maturana and S. Scherer. 2015. VoxNet: A 3D Convolutional Neural Network for Real-Time Object Recognition. In *IROS*.
- Microsoft. 2011–2017. Minecraft. <https://minecraft.net/en-us/>. (2011–2017).
- Max Ogden. 2015. Voxel Builder. <https://github.com/maxogden/voxel-builder>. (2015).
- Charles Ruizhongtai Qi, Hao Su, Matthias Nießner, Angela Dai, Mengyuan Yan, and Leonidas J. Guibas. 2016. Volumetric and Multi-View CNNs for Object Classification on 3D Data. *CoRR* abs/1604.03265 (2016). <http://arxiv.org/abs/1604.03265>
- Danilo Jimenez Rezende, S. M. Ali Eslami, Shakir Mohamed, Peter Battaglia, Max Jaderberg, and Nicolas Heess. 2016. Unsupervised Learning of 3D Structure from Images. *CoRR* abs/1607.00662 (2016). <http://arxiv.org/abs/1607.00662>
- Andrew O. Sageman-Furnas, Nobuyuki Umetani, and Ryan Schmidt. 2015. Meltables: Fabrication of Complex 3D Curves by Melting. In *SIGGRAPH Asia 2015 Technical*

- Briefs (SA '15). ACM, New York, NY, USA, Article 14, 4 pages. DOI: <http://dx.doi.org/10.1145/2820903.2820915>
- Abhishek Sharma, Oliver Grau, and Mario Fritz. 2016. Vconv-dae: Deep volumetric shape learning without object labels. In *Computer Vision-ECCV 2016 Workshops*. Springer, 236–250.
- Nitish Srivastava, Geoffrey Hinton, Alex Krizhevsky, Ilya Sutskever, and Ruslan Salakhutdinov. 2014. Dropout: A Simple Way to Prevent Neural Networks from Overfitting. *J. Mach. Learn. Res.* 15, 1 (Jan. 2014), 1929–1958. <http://dl.acm.org/citation.cfm?id=2627435.2670313>
- Hang Su, Subhransu Maji, Evangelos Kalogerakis, and Erik G. Learned-Miller. 2015. Multi-view convolutional neural networks for 3d shape recognition. In *Proc. ICCV*.
- Jiajun Wu, Chengkai Zhang, Tianfan Xue, William T Freeman, and Joshua B Tenenbaum. 2016. Learning a probabilistic latent space of object shapes via 3d generative-adversarial modeling. In *Advances in Neural Information Processing Systems*. 82–90.
- Zhirong Wu, S. Song, A. Khosla, Fisher Yu, Linguang Zhang, Xiaoou Tang, and J. Xiao. 2015. 3D ShapeNets: A deep representation for volumetric shapes. In *2015 IEEE Conference on Computer Vision and Pattern Recognition (CVPR)*. 1912–1920. DOI: <http://dx.doi.org/10.1109/CVPR.2015.7298801>
- M. E. Yumer and N. J. Mitra. 2016. Learning Semantic Deformation Flows with 3D Convolutional Networks. In *European Conference on Computer Vision (ECCV 2016)*. Springer, –.
- R. Zeleznik, K. Herndon, and J. Hughes. 1996. SKETCH: An Interface for Sketching 3D Scenes. In *ACM SIGGRAPH Computer Graphics (Computer Graphics Proceedings, Annual Conference Series)*. 163–170.
- Y. Zheng, H. Liu, J. Dorsey, and N. J. Mitra. 2016. Ergonomics-Inspired Reshaping and Exploration of Collections of Models. *IEEE Transactions on Visualization and Computer Graphics* 22, 6 (June 2016), 1732–1744. DOI: <http://dx.doi.org/10.1109/TVCG.2015.2448084>
- Jun-Yan Zhu, Philipp Krähenbühl, Eli Shechtman, and Alexei A. Efros. 2016. Generative Visual Manipulation on the Natural Image Manifold. In *Proceedings of European Conference on Computer Vision (ECCV)*.